Performance enhancement of inverted polymer solar cells with fullerene ester derivant-modified ZnO film as cathode buffer layer

Pandeng Li [a,b], Xiaofang Li [a,*], Chunming Sun [b], Guojie Wang [b], Jun Li [b], Tonggang Jiu [b,*], Junfeng Fang [b,*]

[a] School of Chemistry and Chemical Engineering, Hunan University of Science and Technology, Xiangtan, Hunan 411201, PR China
[b] Institute of New Energy Technology, Ningbo Institute of Material Technology and Engineering (NIMTE), Chinese Academy of Science (CAS), Ningbo, Zhejiang 315201, PR China

ARTICLE INFO

Keywords:
ZnO nanoparticles
Fullerene ester derivant
Interfacial modification
Cathode buffer layer
Inverted solar cells

ABSTRACT

In this paper, we reported that ZnO nanoparticles (NPs) film modified with C_{60} pyrrolidine tris-acid ethyl ester (PyC_{60}) was used as cathode buffer layer in inverted polymer solar cells. The resultant device with a blend of PTB7:$PC_{71}BM$ as photoactive materials exhibited an open-circuit voltage (V_{oc}) of 0.753 V, a short-circuit current (J_{sc}) of 16.04 mA cm^{-2}, a fill factor (*FF*) of 72.5%, and an overall power conversion efficiency (PCE) of 8.76%. It was higher than the control devices based on sole ZnO NPs film or ZnO: PyC_{60} hybrid film as cathode buffer layer. It was found that the morphology improvement of ZnO/PyC_{60} film contributed to reducing series loss and interfacial charge recombination. In addition, it improved the interfacial contact with photoactive layer. The results increased electron injection and collection efficiency, and improved *FF*.

1. Introduction

Recently, the polymer solar cells (PSCs) have been extensively studied due to their mechanical flexibility, lightness, and ease of large-area fabrication [1–3]. The power conversion efficiency (PCE) of polymer solar cells has surpassed 10%, which demonstrates their significant applicable potential in the future [4]. It is well known that two main structures of organic solar cells (OSCs) have been developed for single junction device, including the conventional forward device structure and the inverted device structure. Compared to the forward structure which has been widely investigated, the inverted device structure gradually received more attentions in recent years since it makes the PSCs long-term stable [5–9].

To restrain charge recombination and enhance electron collection in inverted PSCs, the key point is to find the favorable cathode buffer layer materials on top of ITO electrode. Among many n-type metal oxides, the solution-processed ZnO NPs are promising candidate for cathode buffer layer due to its relatively high electron mobility, favorable environmental friendliness and stability and high transparency. Therefore ZnO has been intensively exploited in the inverted device [10,11]. However, ZnO buffer layer has several problematic issues such as surface roughness, leakage currents, interfacial recombination and so on. The major concerns with ZnO buffer layer lie in the surface defects and the aggregation of ZnO NPs, which result in relatively low photovoltaic performance [12,13]. So more efforts should be made to modify the ZnO buffer layer and develop low-defect and uniform ZnO film so as to realize high-efficiency inverted PSCs.

In recent literatures, many methods have been applied to modify the ZnO film in the PSCs. In addition to doping metal nanoparticles into ZnO film to improve charge carrier mobility [14,15], one method is adding the polymers or organic small molecules into the ZnO solution to prepare hybrid film [13,16,17]. By this means, the voids of ZnO film can be filled in and the defects of ZnO NPs are passivated. But the incompatible nature of organic molecule with metal oxides limits these applications. Therefore, one modified strategy is implemented by coating a thin self-assembled layer on the surface of ZnO layer such as carboxylic acid-functionlized fullerene [18,19] or conjugated polyelectrolyte [5]. It can fill the surface traps to improve electronic coupling of the ZnO/organic layer, so as to improve J_{sc} and *FF*.

The fullerene derivatives are commonly used as electron-accepting materials in OSCs due to their high electron mobility, good solubility and the preferable compatibility with the electron-donating materials [20–23]. Meanwhile, when the fullerene derivatives are used as cathode buffer layers, they could reduce the series resistance (R_s) of device and improve electron injection and collection. This eventually improves the *FF* and the J_{sc} [8,24,25] by

* Corresponding authors.
E-mail addresses: lixiaofang@iccas.ac.cn (X. Li), jiutonggang@nimte.ac.cn (T. Jiu), fangjf@nimte.ac.cn (J. Fang).

decreasing the electron injection barrier between photoactive layer and electrode. Furthermore, C_{60}-based self-assembled monolayer (SAM) formed onto ZnO NPs film has been systematically investigated in the OSCs [26]. These modifiers serve multiple advantages, such as passivating surface charge traps to improve forward charge transfer, tuning the energy level offset and making up the upper organic layer morphology [27,28]. However, due to the acidic nature of the phosphonic anchoring group, the erosion of the ZnO surface could induce potential device degradation, resulting in poor device performance. So the C_{60}-based modifiers with less-acidic binding units have been explored [12,29,30]. In addition, the modifiers with ester units possess much weaker acidity and have affinity to metal oxide surfaces [26]. Moreover, the fullerenes with ester units have non-covalent interaction with the other π-conjugated molecules and retain the high electron mobility [22,31,32].

Herein, we demonstrate high-efficiency inverted PSCs with ZnO NPs modified by PyC_{60} as the cathode buffer layer. The inverted device achieves the PCE of 8.76% based on a blend of Poly[[4,8-bis[(2-ethylhexyl)oxy]benzo-[1,2-b:4,5-b′] dithiophene-2,6-diyl][3-fluoro-2-[(2-ethylhexyl)-carbonyl]-thieno-[3,4-b]thiophenedi-yl]] (PTB7) and (6,6)-phenyl C71-butyric acid methyl ester ($PC_{71}BM$). It is higher than those of the devices based on sole ZnO buffer layer and ZnO: PyC_{60} hybrid buffer layer. To figure out the reason of PCE improvement, the energy level property, optoelectronic properties, surface morphology of the ZnO/PyC_{60} film have been fully investigated. It is found that the film morphology of ZnO/PyC_{60} and the contact quality between ZnO/PyC_{60} and photoactive layer are improved. It leads to the increment in both V_{oc} and *FF*, giving the high photovoltaic performance.

2. Experimental section

2.1. Reagent and materials

Indium tin oxide (ITO) coated glass substrates were bought from CSG HOLDING CO., LTD (China) ($R_s \leq 10\ \Omega/\square$ and $T_r \geq 83\%$). Electron acceptor material $PC_{71}BM$ was purchased from ADS. And electron donor material PTB7 was purchased from 1-material Chemscitech. PyC_{60} and chlorobenzene were obtained from Sigma-Aldrich.

2.2. Preparation of the ZnO NPs and PyC_{60} solution

ZnO nanoparticles were synthesized according to the procedures [33,34]. We used the mixed solvent (methanol:chloroform = 2:1 V/V) to disperse the nanoparticles to obtain a sol with, on average, 15 mg mL^{-1} ZnO. The PyC_{60} solutions with different concentrations were prepared by dissolving the PyC_{60} with the chloroform. The hybrid buffer layer was obtained from spin-coating blend solution (ZnO NPs and PyC_{60}) with weight ratio (10:2 mg mL^{-1}). The blend solution was prepared by mixing the respective solutions of ZnO NPs (15 mg mL^{-1}) and PyC_{60} (10 mg mL^{-1}).

2.3. Device fabrication and characterization

The inverted PSCs herein have a structure of ITO/(ZnO/PyC_{60} or ZnO NPs or ZnO: PyC_{60})/PTB7:$PC_{71}BM$/MoO_3/Al. The devices were fabricated on ITO-coated glass substrates which were cleaned by sequential ultrasonic baths of detergent, deionized water, acetone and isopropanol. The substrates were dried with nitrogen stream and then exposed to UV–ozone for 30 min. The ZnO film annealed at 80 °C for 10 min, giving the thickness of 25 nm. To modify ZnO film, the PyC_{60} solutions were spin-coated on ZnO film at 2500 rpm for 60 s and the resultant ZnO/PyC film was placed under the vacuum for 10 min. The photoactive layer of PTB7: $PC_{71}BM$ (10:8 in weight ratio) was prepared via spin-coating from chlorobenzene solution at 2000 rpm for 120 s. Finally the device fabrication was completed by thermal evaporation of 10 nm of MoO_3 and 100 nm of Al under vacuum with a base pressure of 1×10^{-6} mbar. The device area was 0.04 cm^2. The *J–V* characteristics were measured with a Keithley 2400 source measure unit under AM 1.5G irradiation (100 mW cm^{-m}).

2.4. Cathode buffer layers characterization

Optical transmittance spectra were measured in a UV-3300 spectrophotometer. The surface morphology and the film roughness of the specimens were characterized by scanning electron microscopy (SEM) operated at an acceleration voltage of 8 kV (S-4800). Atomic force microscope (AFM) measurements were operated in tapping mode using a Veeco dimension V atomic microscope. Scanning Kelvin probe microscopy (SKPM) measurements were carried out on an AFM equipment with the standard SKPM mode. The external quantum efficiency (EQE) was performed by the IQE200TM data acquisition system.

3. Results and discussion

3.1. Photovoltaic device structure and energy level diagram

The inverted device structure is shown in Fig. 1a along with the chemical structure of PyC_{60} which has three ester groups. To visualize the energy level relationship of photoactive materials as well as ZnO/PyC_{60} film, cyclic voltammetry (CV) was carried out to investigate the electrochemical properties of PyC_{60} and $PC_{71}BM$ (see Fig. S1 in the Supporting information). The lowest unoccupied molecular orbital (LUMO) and the highest occupied molecular orbital (HOMO) of PyC_{60} are −4.14 eV and −5.83 eV, respectively. The energy levels of $PC_{71}BM$ are also determined as −4.04 eV and −5.74 eV, respectively. The electronic energy levels of PTB7 and MoO_3 were obtained from the literatures [9,35]. Fig. 1b displays the corresponding energy level diagram of the components in the device. It is obvious that the LUMO level of PyC_{60} is just in between

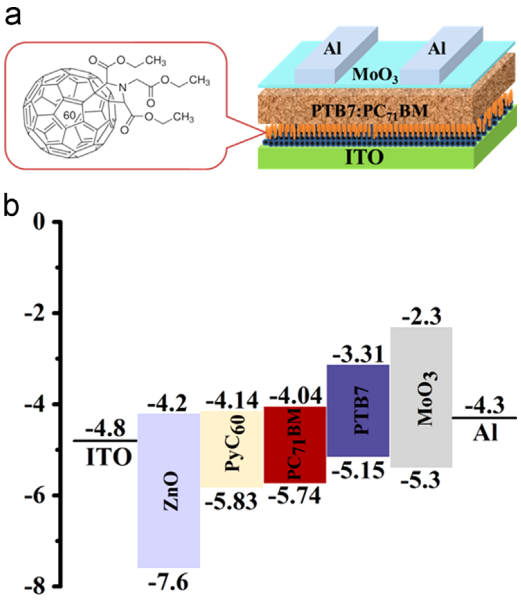

Fig. 1. (a) Device structure of the inverted PSCs with the bilayer film of ZnO/PyC_{60} as cathode buffer layer. (b) The corresponding energy level diagram of the components of the device.

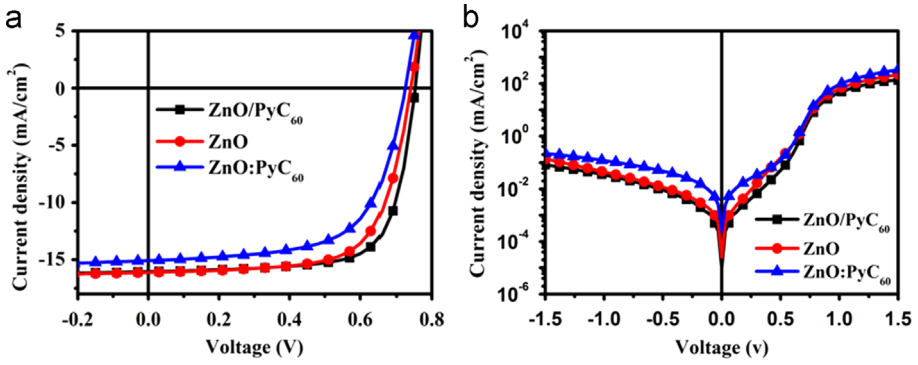

Fig. 2. (a) Illuminated and (b) dark *J–V* characteristics of PTB7:$PC_{71}BM$ devices with different cathode buffer layers.

Table 1
Summary of the photovoltaic parameters of PTB7:$PC_{71}BM$ devices fabricated with different cathode buffer layers. The rectification ratio (*RR*, defined as the ratio of the forward-to-reverse bias current density at a bias voltage of ± 1.5 *V*) was obtained from dark *J–V* characteristics.

Interlayer	V_{oc} [V]	J_{sc} [mA cm^{-2}]	*FF* [%]	*PCE* [%] Best/average[a]	R_s [Ω cm^2]	R_{sh} [kΩ cm^2]	*RR* [dark]
ZnO/PyC_{60}	0.753	16.04	72.5	8.76/8.62	3.32	1.42	1591
ZnO	0.740	16.11	68.5	8.17/7.92	5.36	1.29	1570
ZnO: PyC_{60}	0.725	15.07	64.2	7.01/6.03	5.48	0.77	1522

[a] The parameters of devices are averaged by seven devices. The device parameters distribution maps are presented in Fig. S2.

those of the $PC_{71}BM$ and ZnO, building the preferable energy level cascade. So the electrons can be easily transferred from $PC_{71}BM$ to ITO electrode without much energy loss. Moreover, the HOMO level of PyC_{60} (-5.83 eV) is lower than those of PTB7 (-5.15 eV) and $PC_{71}BM$ (-5.74 eV), blocking the hole transport from PTB7 to the ITO electrode.

3.2. Devices with different cathode buffer layers

The *J–V* characteristics of the devices with different cathode buffer layers under AM 1.5G irradiation are depicted in Fig. 2a, and the extracted parameters are summarized in Table 1. It can be observed that the ZnO/PyC_{60} based device shows the best PCE of 8.76% with a V_{oc} of 0.753 V, a J_{sc} of 16.04 mA cm^{-2}, and a *FF* of 72.5%. As control, the device with ZnO buffer layer shows V_{oc} of 0.740 V, J_{sc} of 16.11 mA cm^{-2} and *FF* of 68.5%, giving the relatively low PCE of 8.17%. Meanwhile, the ZnO: PyC_{60} film based device also presents low PCE of 7.01%. In addition, the device based on sole PyC_{60} buffer layer could not support any device parameters due to poor surface morphology. Moreover, the series resistance (R_s) of the ZnO/PyC_{60} based device is 3.32 Ω cm^2, much lower than those of the devices with ZnO (5.36 Ω cm^2) and ZnO: PyC_{60} (5.48 Ω cm^2), and the shunt resistance (R_{sh}, 1.42 kΩ cm^2) of ZnO/PyC_{60} based device is higher than those of ZnO based device (1.29 kΩ cm^2) and ZnO: PyC_{60} based device (0.77 kΩ cm^2). The results suggest that the incorporation of PyC_{60} modified layer can lead to a simultaneous enhancement of V_{oc} and *FF* in contrast to the controlled devices.

3.3. Electrical characteristics of different cathode buffer layers

To further probe the electrical characteristics of the inverted devices, the *J–V* characteristics were measured in the dark and shown in Fig. 2b. The ZnO/PyC_{60} based device exhibits favorable diode characteristics with a low leakage current and a high rectification ratio (see Table 1). Hence, according to the Shockley equation and the model of Mihailetchi et al. [36,37], a slightly higher V_{oc} can be expected and reached 0.753 V. In addition, the R_s of the ZnO/PyC_{60} based device is much lower than those of the devices with ZnO and ZnO: PyC_{60}. Those results indicate that the good electrical properties of ZnO/PyC based device, such as a low R_s and a high R_{sh}, are responsible for the increment of device performances [38].

3.4. Light transmission and EQE curves of different buffer cathode layers

The transmittance of cathode buffer layer is very important to influence the penetrability of incident light from ITO side. The optical transmittance spectra of ZnO/PyC_{60} film and the controlled ZnO film are shown in Fig. 3a. The transmittance of ZnO/PyC_{60} is almost the same as that of the ZnO film in the wavelength region of 650–900 nm. However, the transmittance in region of 350–650 nm is gradually reduced because of the absorption of PyC_{60} (see Fig. S3 in the Supporting information), it would lower light absorption of the photoactive layer and thus lead to the reduced photocurrent. Fig. 2b presents EQE spectra of the devices. It is apparent that the EQE of the ZnO/PyC_{60} based device is slightly higher than that of the ZnO based device in the wavelength region of 350–550 nm. The possible reason for the contradiction of the transmittance and the EQE is that the absorption of ZnO/PyC_{60} film may generate the photocurrent. In addition, the direct contact of PyC_{60} and photoactive layer may enhance internal photoelectron conversion efficiency by reducing the electron injection barrier between photoactive layer and ZnO film, which is also responsible for the increase of EQE [24,39]. On the other hand the EQE of the ZnO/PyC_{60} based device is decreased compared to the ZnO based device in the region of 650–700 nm. Therefore, the J_{sc} of the ZnO/PyC_{60} based device is very close to that of the ZnO based device.

3.5. Surface morphology of different cathode buffer layers

To scrutinize the morphology change effect on device performance, Fig. 4 displays the SEM images and AFM images of ZnO/PyC_{60} film together with controlled ZnO NPs film. The root-mean-square (rms) roughness of ZnO film is 2.26 nm and large amounts of voids exist in the surface of ZnO film shown in Fig. 4a and c. The poor film morphology would lead to leakage current. With the insertion of PyC_{60} modified layer, the roughness (1.24 nm) of ZnO film is effectively decreased and the voids are filled in. As a result,

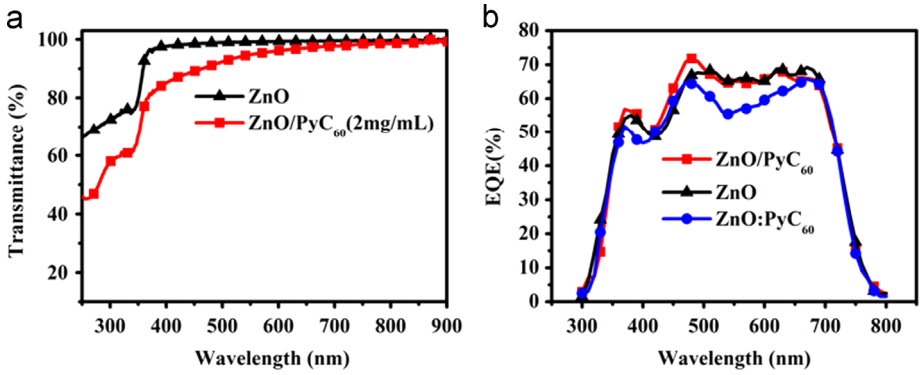

Fig. 3. (a) UV–visible transmittance spectra of ZnO film, and ZnO/PyC_{60} bilayer film and (b) EQE data of device based on PTB7:$PC_{71}BM$ blends using different buffer layers.

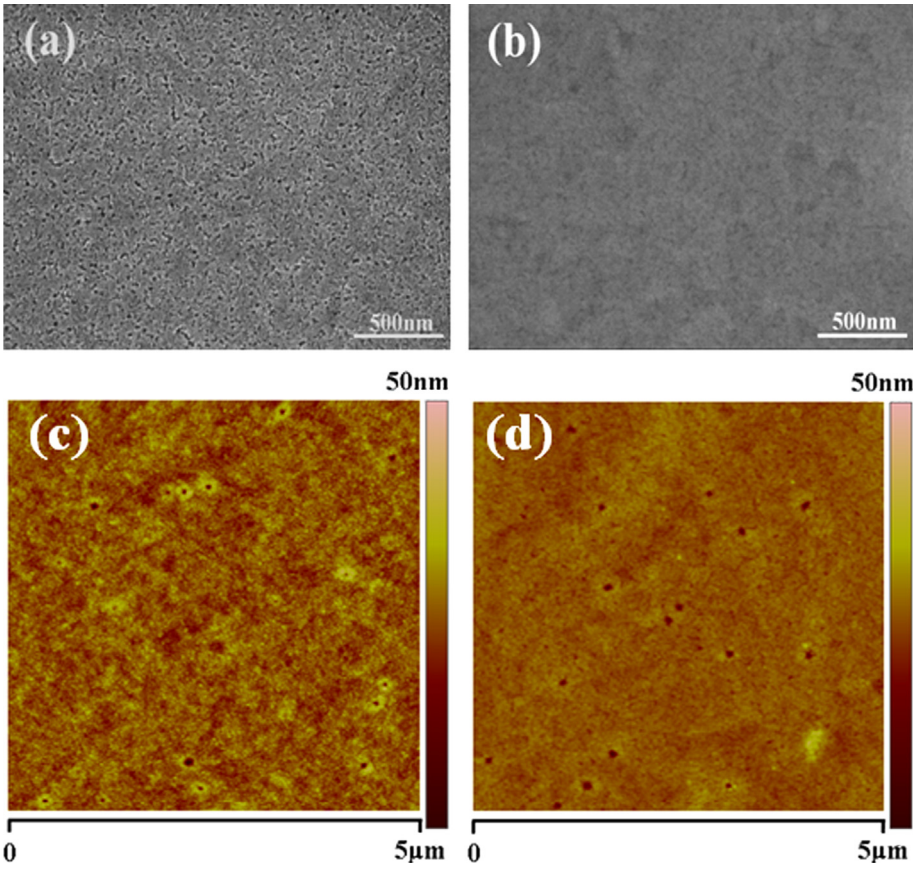

Fig. 4. SEM images of (a) ZnO NPs and (b) ZnO/PyC_{60} (scale bar: 500 nm) and AFM images of the topological morphology of (c) ZnO NPs and (d) ZnO/PyC_{60} (a scan size of $5 \times 5\ \mu m^2$).

the ZnO/PyC_{60} film shows smooth and more compact surface morphology as evidenced by Fig. 4b and d. However, the large roughness and aggregation can be obviously found in Fig. S4 for hybrid buffer layer. The ZnO film and the ZnO: PyC_{60} hybrid film undoubtedly increase leakage current and result in low *FF* in the devices. The results indicate that the ZnO/PyC_{60} film with preferable surface morphology reduces leakage current and interfacial charge recombination [13]. This is in good agreement with the results obtained from dark *J–V* characteristics.

3.6. *Surface potential and photoluminescence of PyC_{60}-modified ZnO film*

In addition, the surface potential was directly examined by KPFM (see Fig. S5 in the Supporting information). The measurement of ZnO/PyC film obtained a 261 mV shift in average surface potential compared to that of ZnO film. The differences in surface potential demonstrate that the microscopic electric dipole between the ZnO/PyC_{60} film and photoactive layer lowers the electron injection barrier. This can promote electron injection and reduce contact resistance with the photoactive layer [24,40]. In addition, the surface potential was also influenced by the electronic states of film surface such as surface traps, surface reconstruction, chemical composition, etc. [41,42]. The modification of ZnO film by the PyC_{60} was studied by photoluminescence (PL) as well. As shown in Fig. S6, the emission band of ZnO film at 528 nm has been well known as an indicator of the defect states in ZnO NPs [43,44]. It is noticed that the defect emission becomes weaker when the ZnO film is modified by the PyC_{60}. The decrease of defect emission is probably because the surface traps are reduced, resulting in reduced interfacial charge recombination. Another reason for the decrease is that the defect emission is partly absorbed by PyC_{60}. Therefore the decrease of defect emission may be the integration from

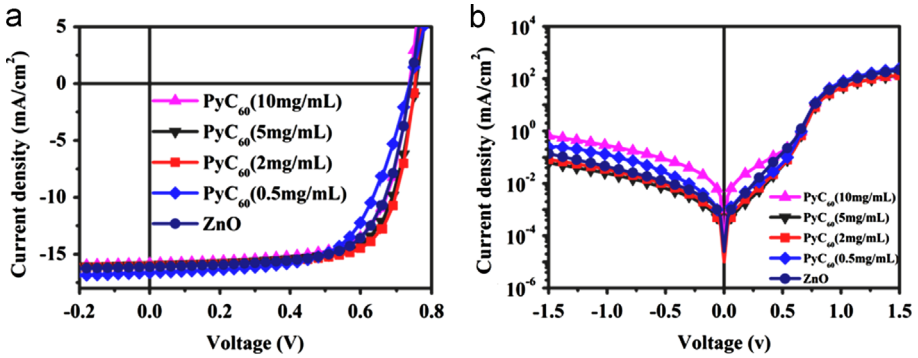

Fig. 5. (a) Illuminated and (b) dark *J–V* characteristics of PTB7:$PC_{71}BM$ devices operated with different PyC_{60} concentration.

Table 2
Summary of device performances with different PyC_{60} concentrations.

Concentration (mg mL^{-1})	V_{oc} [V]	J_{sc} [mA cm^{-2}]	*FF* [%]	*PCE* [%] Best/average[a]	R_s [Ω cm^2]	R_{sh} [kΩ cm^2]
10	0.737	15.82	69.6	8.11/8.07	4.48	1.14
5	0.755	15.91	70.9	8.52/8.44	4.60	1.31
2	0.753	16.04	72.5	8.76/8.62	3.32	1.42
0.5	0.728	16.59	66.8	8.07/6.65	4.68	0.91
0	0.740	16.11	68.5	8.17/7.92	5.36	1.29

[a] The parameters of devices are averaged by seven devices.

the reduction of surface defect of ZnO NPs and optical absorption of PyC_{60}. Since the defect emission band of ZnO/PyC_{60} film is only slightly weaker than that of ZnO film which means most surface defects of ZnO NPs still retain, we conclude that the optical absorption of PyC_{60} is mainly responsible for the weakening of defect emission. In this case, the increment of surface potential of ZnO/PyC_{60} film might originate from the preferable surface morphology and the diminishment of surface traps, resulting in reducing charge recombination [45].

3.7. *Thickness effect of PyC_{60} on the device performances*

To figure out the thickness effect on device performance, *J–V* characteristics of photovoltaic devices with different PyC_{60} concentrations are depicted in Fig. 5 and the detailed parameters are summarized in Table 2. As can be seen, when PyC_{60} concentration decreases from 10 mg mL^{-1} to 2 mg mL^{-1}, the V_{oc}, J_{sc} and *FF* of the devices are all improved and consequently result in enhancement of PCE (8.62% in average). Meanwhile, the device shows a smallest R_s (3.32 Ω cm^2) and a highest R_{sh} (1.42 KΩ cm^2) at the concentration of 2 mg mL^{-1}. The higher PyC_{60} concentration gives thicker PyC_{60} film, which fills the surface voids of ZnO film. However it increases interfacial resistance and lowers light transmittance of interfacial film, influencing device performance negatively. So the performance is getting better with the PyC_{60} concentration decreasing. Furthermore, as the PyC_{60} concentration is further reduced to 0.5 mg mL^{-1}, the device parameters show that the J_{sc} is improved, while the V_{oc} and the *FF* are obviously decreased, giving an average PCE of 6.65%. The lower PyC_{60} concentration improves light transmittance of the ZnO/PyC_{60} film, while does not effectively fill in the surface voids and finally leads to leakage current [46]. So the optimal concentration of the PyC_{60} is 2 mg mL^{-1} and then the optimized ZnO/PyC_{60} film (about 32 nm) for preferable device performance can be achieved. Fig. 5b shows the dark *J–V* characteristic of devices with different PyC_{60} concentration. It is clear that the device using optimal PyC_{60} concentration has favorable diode characteristics and shows low leakage current. Meanwhile, the EQE curves of different PyC_{60} concentrations are shown in Fig. S7. The tendency of EQE curves is in good agreement with the *J* data in Table 2. These results indicate that the suitable thickness of interfacial modified layer could effectively improve the device performance.

3.8. *Stability study of devices*

In contrast to conventional forward configuration, the inverted configuration with ZnO cathode buffer layer exhibited significantly superior long-term stability [47]. To investigate the effect of ZnO/PyC_{60} film on the stability of device, the PCE degradation of devices based on ZnO/PyC_{60} and ZnO was tested over time at argon condition. As shown in Fig. S8, the PCE of device based on ZnO/PyC_{60} decays only 11.3% of the original value after storage for 22 days, which is slightly better to that of device based on ZnO (12.8%) in the same condition. This indicates that PyC_{60}-modified ZnO film as cathode buffer layer is beneficial for the long-term stability of the device.

4. Conclusion

In summary, we have successfully developed a double layer as cathode buffer layer via ZnO film modified by the PyC_{60} upper layer, with which high-efficiency inverted PSCs based on a blend of PTB7:$PC_{71}BM$ as photoactive layer are achieved, giving the average efficiency of 8.62%. The PyC_{60} fills in the voids of ZnO film and partly passivates the defects of ZnO NPs to improve the morphology quality of ZnO/PyC_{60} film. Moreover, the interfacial contact between the ZnO and photoactive layer is improved, lowering the electron injection barrier. In this way, the ZnO/PyC_{60} cathode buffer layer not only decreases series loss and interfacial charge recombination, but also increases electron injection and collection efficiency, which lead to the high device performance. In the meantime, the device shows good device stability after PyC_{60} modification.

Acknowledgments

The authors gratefully acknowledge the support of the National Natural Science Foundation of China (Nos. 51202264 and 51273208), and the Specialized Research Fund for the Spring Buds Talent Program (No. Y20804RA02). The work was also supported by Zhejiang Provincial Natural Science Foundation of China; the Starting Research Fund of Team Talent (Y10801RA01) in NIMTE.

Appendix A. Supporting information

Supporting information associated with this article can be found in the online version at http://dx.doi.org/10.1016/j.solmat.2014.03.038.

References

[1] J. Chen, Y. Cao, Development of novel conjugated donor polymers for high-efficiency bulk-heterojunction photovoltaic devices, Acc. Chem. Res. 42 (2009) 1709–1718.

[2] F.C. Krebs, T. Tromholt, M. Jørgensen, Upscaling of polymer solar cell fabrication using full roll-to-roll processing, Nanoscale 2 (2010) 873–886.

[3] W. Cai, X. Gong, Y. Cao, Polymer solar cells: recent development and possible routes for improvement in the performance, Sol. Energy Mater. Sol. Cells 94 (2010) 114–127.

[4] J. You, L. Dou, K. Yoshimura, T. Kato, K. Ohya, T. Moriarty, K. Emery, C.-C. Chen, J. Gao, G. Li, Y. Yang, A polymer tandem solar cell with 10.6% power conversion efficiency, Nat. Commun. 4 (2013) 1–10.

[5] Y.M. Chang, C.Y. Leu, Conjugated polyelectrolyte and zinc oxide stacked structure as an interlayer in highly efficient and stable organic photovoltaic cells, J. Mater. Chem. A 1 (2013) 6446–6451.

[6] M. Jørgensen, K. Norrman, S.A. Gevorgyan, T. Tromholt, B. Andreasen, F.C. Krebs, Stability of polymer solar cells, Adv. Mater. 24 (2012) 580–612.

[7] L.-M. Chen, Z. Hong, G. Li, Y. Yang, Recent progress in polymer solar cells: manipulation of polymer: fullerene morphology and the formation of efficient inverted polymer solar cells, Adv. Mater. 21 (2009) 1434–1449.

[8] Z. Xu, L.-M. Chen, G. Yang, C.-H. Huang, J. Hou, Y. Wu, G. Li, C.-S. Hsu, Y. Yang, Vertical phase separation in poly(3-hexylthiophene): fullerene derivative blends and its advantage for inverted structure solar cells, Adv. Funct. Mater. 19 (2009) 1227–1234.

[9] Z. He, C.Z.S. Su, M. Xu, H. Wu, Y. Cao, Enhanced power-conversion efficiency in polymer solar cells using an inverted device structure, Nat. Photonics 190 (2012) 591–595.

[10] Y. Sun, J.H. Seo, C.J. Takacs, J. Seifter, A.J. Heeger, Inverted polymer solar cells integrated with a low-temperature-annealed sol–gel-derived zno film as an electron transport layer, Adv. Mater. 23 (2011) 1679–1683.

[11] M.S. White, D.C. Olson, S.E. Shaheen, N. Kopidakis, D.S. Ginley, Inverted bulk-heterojunction organic photovoltaic device using a solution-derived ZnO underlayer, Appl. Phys. Lett. 89 (2006) 143517.

[12] S.K. Hau, H.-L. Yip, H. Ma, A.K.-Y. Jen, High performance ambient processed inverted polymer solar cells through interfacial modification with a fullerene self-assembled monolayer, Appl. Phys. Lett. 93 (2008) 233304.

[13] S. Shao, K. Zheng, T. Pullerits, F. Zhang, Enhanced performance of inverted polymer solar cells by using poly(ethylene oxide)-modified ZnO as an electron transport layer, ACS Appl. Mater. Interfaces 5 (2013) 380–385.

[14] A. Gadisa, Y. Liu, E.T. Samulski, R. Lopez, Role of thin n-type metal-oxide interlayers in inverted organic solar cells, ACS Appl. Mater. Interfaces 4 (2012) 3846–3851.

[15] V. Bhosle, J.T. Prater, F. Yang, S.R. Forrest, D. Burk, J. Narayan, Gallium-doped zinc oxide films as transparent electrodes for organic solar cell applications, J. Appl. Phys. 102 (2007) 023501.

[16] C.E. Small, S. Chen, J. Subbiah, C.M. Amb, S.-W. Tsang, T.-H. Lai, J.R. Reynolds, F. So, High-efficiency inverted dithienogermole–thienopyrrolodione-based polymer solar cells, Nat. Photonics 6 (2012) 115–120.

[17] T. Hu, F. Li, K. Yuan, Y. Chen, Efficiency and air-stability improvement of flexible inverted polymer solar cells using ZnO/poly(ethylene glycol) hybrids as cathode buffer layers, ACS Appl. Mater. Interfaces 5 (2013) 5763–5770.

[18] T. Stubhan, M. Salinas, A. Ebel, F.C. Krebs, A. Hirsch, M. Halik, C.J. Brabec, Increasing the fill factor of inverted P3HT:PCBM solar cells through surface modification of Al-doped ZnO via phosphonic acid-anchored C60 SAMs, Adv. Funct. Mater. 2 (2012) 532–535.

[19] Y.-J. Cheng, C.-H. Hsieh, Y. He, C.-S. Hsu, Y. Li, Combination of indene-C_{60} bis-adduct and cross-linked fullerene interlayer leading to highly efficient inverted polymer solar cells, J. Am. Chem. Soc. 132 (2010) 17381–17383.

[20] P.A. Troshin, H. Hoppe, J. Renz, M. Egginger, J.Y. Mayorova, A.E. Goryachev, A.S. Peregudov, R.N. Lyubovskaya, G. Gobsch, N.S. Sariciftci, V.F. Razumov, Material solubility–photovoltaic performance relationship in the design of novel fullerene derivatives for bulk heterojunction solar cells, Adv. Funct. Mater. 19 (2009) 779–788.

[21] C.J. Brabec, A. Cravino, D. Meissner, N.S. Sariciftci, T. Fromherz, M.T. Rispens, L. Sanchez, J.C. Hummelen, Origin of the open circuit voltage of plastic solar cells, Adv. Funct. Mater. 11 (2001) 374–380.

[22] S. Gunes, H. Neugebauer, N.S. Sariciftci, Conjugated polymer-based organic solar cells, Chem. Rev. 107 (2007) 1324–1338.

[23] C. Yang, J.Y. Kim, S. Cho, J.K. Lee, A.J. Heeger, F. Wudl, Functionalized methanofullerenes used as n-type materials in bulk-heterojunction polymer solar cells and in field-effect transistors, J. Am. Chem. Soc. 130 (2008) 6444–6450.

[24] Q. Wei, T. Nishizawa, K. Tajima, K. Hashimoto, Self-organized buffer layers in organic solar cells, Adv. Mater. 20 (2008) 2211–2216.

[25] X. Li, W. Zhang, Y. Wu, C. Min, J. Fang, High performance polymer solar cells with a polar fullerene derivative as the cathode buffer layer, J. Mater. Chem. A 1 (2013) 12413–12416.

[26] S.K. Hau, Y.-J. Cheng, H.-L. Yip, Y. Zhang, H. Ma, A.K.-Y. Jen, Effect of chemical modification of fullerene-based self-assembled monolayers on the performance of inverted polymer solar cells, ACS Appl. Mater. Interfaces 2 (2010) 1892–1902.

[27] C.-H. Hsieh, Y.-J. Cheng, P.-J. Li, C.-H. Chen, M. Dubosc, R.-M. Liang, C.-S. Hsu, Highly efficient and stable inverted polymer solar cells integrated with a cross-linked fullerene material as an interlayer, J. Am. Chem. Soc. 132 (2010) 4887–4893.

[28] S.K. Hau, H.-L. Yip, O. Acton, N.S. Baek, H. Ma, A.K.-Y. Jen, Interfacial modification to improve inverted polymer solar cells, J. Mater. Chem. 18 (2008) 5113–5119.

[29] B.A. Borgias, S.R. Cooper, Y.B. Koh, K.N. Raymond, Synthetic, structural, and physical studies of titanium complexes of catechol and 3,5-di-tert-butylcatechol, Inorg. Chem. 23 (1984) 1009–1016.

[30] J. Moser, S. Punchihewa, P.P. Infelta, M. Gratzel, Surface complexation of colloidal semiconductors strongly enhances interfacial electron-transfer rates, Langmuir 7 (1991) 3012–3018.

[31] S. Mukherjee, A.K. Bauri, S. Bhattacharya, Determination of binding strength for the supramolecular complexation of a designed bisporphyrin with C_{60}, C_{70} and their derivatives employing absorption spectrophotometric, fluorescence and quantum chemical calculations, Spectrochim. Acta Part A 79 (2011) 1952–1958.

[32] S. Mukherjee, A.K. Bauri, S. Bhattacharya, Photophysical investigations on determination of molecular structure and binding strength of supramolecular complexation between fulleropyrrolidine and a designed bisporphyrin in solution, Spectrochim. Acta Part A 109 (2013) 32–36.

[33] C. Pacholski, A. Kornowski, H. Weller, Self-assembly of ZnO: from nanodots to nanorods, Angew. Chem. Int. Ed. 41 (2002) 1188–1191.

[34] W.J.E. Beek, M.M. Wienk, M. Kemerink, X. Yang, R.A.J. Janssen, Hybrid zinc oxide conjugated polymer bulk heterojunction solar cells, J. Phys. Chem. B 109 (2005) 9505–9516.

[35] C. Tao, S. Ruan, X. Zhang, G. Xie, L. Shen, X. Kong, W. Dong, C. Liu, W. Chen, Performance improvement of inverted polymer solar cells with different top electrodes by introducing a MoO_3 buffer layer, Appl. Phys. Lett. 93 (2008) 193307.

[36] C. He, C. Zhong, H. Wu, R. Yang, W. Yang, F. Huang, G.C. Bazan, Y. Cao, Origin of the enhanced open-circuit voltage in polymer solar cells via interfacial modification using conjugated polyelectrolytes, J. Mater. Chem. 20 (2010) 2617–2622.

[37] V.D. Mihailetchi, P.W.M. Blom, J.C. Hummelen, M.T. Rispens, Cathode dependence of the open-circuit voltage of polymer:fullerene bulk heterojunction solar cells, J. Appl. Phys. 94 (2003) 6849–6854.

[38] Z. Liang, Q. Zhang, O. Wiranwetchayan, J. Xi, Z. Yang, K. Park, C. Li, G. Cao, Effects of the morphology of a ZnO buffer layer on the photovoltaic performance of inverted polymer solar cells, Adv. Funct. Mater. 22 (2012) 2194–2201.

[39] W. Zhang, M. Saliba, S.D. Stranks, Y. Sun, X. Shi, U. Wiesner, A.H.J. Snaith, Enhancement of perovskite-based solar cells employing core–shell metal nanoparticles, Nano Lett. 13 (2013) 4505–4510.

[40] Z. He, C. Zhong, X. Huang, W.-Y. Wong, H. Wu, L. Chen, S. Su, Y. Cao, Simultaneous enhancement of open-circuit voltage, short-circuit current density, and fill factor in polymer solar cells, Adv. Mater. 23 (2011) 4636–4643.

[41] M. Nonnenmacher, M.P. O'Boyle, H.K. Wickramasinghe, Kelvin probe force microscopy, Appl. Phys. Lett. 58 (1991) 2921.

[42] L.S.C. Pingree, O.G. Reid, D.S. Ginger, Electrical scanning probe microscopy on active organic electronic devices, Adv. Mater. 21 (2009) 19–28.

[43] A.v. Dijken, E.A. Meulenkamp, D. Vanmaekelbergh, A. Meijerink, Influence of adsorbed oxygen on the emission properties of nanocrystalline zno particles, J. Phys. Chem. B 104 (2000) 4355–4360.

[44] A.v. Dijken, E.A. Meulenkamp, D. Vanmaekelbergh, A. Meijerink, The kinetics of the radiative and nonradiative processes in nanocrystalline ZnO particles upon photoexcitation, J. Phys. Chem. B 104 (2000) 1715–1723.

[45] H. Zhou, Y. Zhang, J. Seifter, S.D. Collins, C. Luo, G.C. Bazan, T.-Q. Nguyen, A.J. Heeger, High-efficiency polymer solar cells enhanced by solvent treatment, Adv. Mater. 25 (2013) 1646–1652.

[46] C.-H. Chou, W.L. Kwan, Z. Hong, L.-M. Chen, Y. Yang, Metal-oxide interconnection layer for polymer tandem solar cells with an inverted architecture, Adv. Mater. 23 (2011) 1282–1286.

[47] A.K.K. Kyaw, D.H. Wang, V. Gupta, J. Zhang, S. Chand, G.C. Bazan, A.J. Heeger, Efficient solution-processed small-molecule solar cells with inverted structure, Adv. Mater. 25 (2013) 2397–2402.